IOPscience iopscience.iop.org

Home Search Collections Journals About Contact us My IOPscience

Characterization of Single-Crystalline Aluminum Thin Film on (100) GaAs Substrate

This content has been downloaded from IOPscience. Please scroll down to see the full text.

2013 Jpn. J. Appl. Phys. 52 045801

(http://iopscience.iop.org/1347-4065/52/4R/045801)

View the table of contents for this issue, or go to the journal homepage for more

Download details:

IP Address: 140.113.38.11
This content was downloaded on 26/04/2014 at 06:58

Please note that terms and conditions apply.

Japanese Journal of Applied Physics 52 (2013) 045801 **REGULAR PAPER**
http://dx.doi.org/10.7567/JJAP.52.045801

Characterization of Single-Crystalline Aluminum Thin Film on (100) GaAs Substrate

Shi-Wei Lin[1], Jau-Yang Wu[1], Sheng-Di Lin[1]*, Ming-Cheng Lo[1], Ming-Huei Lin[1], and Chi-Te Liang[2]

[1] *Department of Electronics Engineering, National Chiao Tung University, Hsinchu 300, Taiwan*
[2] *Department of Physics, National Taiwan University, Taipei 106, Taiwan*
E-mail: sdlin@mail.nctu.edu.tw

Received November 29, 2012; accepted December 29, 2012; published online March 12, 2013

We have studied the structure and physical properties of an aluminum thin film grown on a (100) GaAs substrate. The X-ray diffraction (XRD) data shows that the Al film grown in situ by molecular beam epitaxy (MBE) is single crystalline. Compared with the polycrystalline film ex situ evaporated using an electron-gun (E-gun), the MBE-grown Al film has a high optical reflectivity in the visible and ultraviolet (UV) regime. In addition, the MBE-grown film has a 2-order-lower residue resistance, a 1-order-higher temperature coefficient of resistance, and a 2-order-larger magnetoresistance (MR) than the polycrystalline film. Owing to the long mean free time, the bulk-like electron-to-hole transition of Hall resistivity is observed for the first time in a nanoscale metal thin film. Our results suggest that MBE-grown Al thin films have great potential applications in metal-based nanoelectronics and nanophotonics. © 2013 The Japan Society of Applied Physics

1. Introduction

Metallic films have been a research topic since the early 20th century because of their fundamental importance and extensive application in the modern industry. Thin metal films have broad relevance in the semiconductor industry for electrical and photonic devices. Highly conductive and nanometer-scale metal films are also a key element for interconnects and electrical contact in current integrated-circuit (IC) fabrication and nanophotonics. On the other hand, metallic films are also attractive to researchers in condensed matter physics. Studies of the transport properties of various metal films have been reported. In these reports, metal thin films are generally deposited ex situ using electron gun (E-gun) evaporation, thermal evaporation, or sputtering techniques on a crystallized or noncrystallized substrate at room temperature or cryotemperature.[1–8] However, it is difficult to obtain a coherent sense among the reported data quantitatively because the physical properties of deposited films strongly depend on the deposition conditions. Therefore, it could be very helpful if one can instead study, either optically or electrically, the physical properties of a single-crystalline metal film. Very recently, single-crystalline metal has also become a key element in fabricating plasmonic/nanophotonics devices and circuits.[9] Huang et al. demonstrated that, to make high-definition optical antennas reproducible, the crystal quality of metal thin films plays an essential role.[10] On the other hand, by using single-crystalline silver, the performance and operating temperature of nanolasers has been significantly improved owing to the reduced loss of metal films.[11]

There are two reasons for the random or poor quality of metal thin films. The first one is the presence of incorporated impurities that are related to the purity of the evaporated source and the cleanness of the chamber environment. The other one is the order of crystal structure. It is not possible to grow single-crystal metal films if the substrate/template used is not a single crystal. Even if a single-crystal substrate is used, matching the crystal structures and lattice constants between the substrate and the metal thin film is also a daunting challenge. The oxidation of the interface between the metal and the substrate is also a problem owing to unavoidable exposure to air before metal evaporation. Therefore, the deposition usually forms polycrystalline or amorphous metal films as previously reported. In this work, we use in situ molecular beam epitaxy (MBE) to solve these problems. By using an ultrahigh-vacuum (UHV) chamber and high-purity sources, the fabrication can be accomplished in a nearly impurity-free environment. Previous studies showed that it is possible to grow single-crystalline aluminum thin films on a GaAs(100) substrate, although the growth mechanism and favored crystal orientation are still under debate.[12–16] Surprisingly, although the optical and transport properties of grown Al films are of interest for various applications, they have not yet been systematically studied. We therefore investigate the structure and physical properties of single-crystalline aluminum films grown on a (100) GaAs substrate. Samples prepared by conventional E-gun evaporation are also characterized for comparison. X-ray diffraction (XRD) analysis and atomic force microscopy (AFM) are used to study the crystallization and surface morphology, respectively. The optical reflectivity spectra are measured to characterize the optical properties of the thin films. The measurements of electrical resistivity, Hall coefficient, and magnetoresistance are also carried out to understand the transport properties of the thin films.

2. Experimental Procedure

Several samples with film thicknesses in the range of 30–100 nm were studied but with focus on two representative samples for clarity. Two 60-nm-thick Al films on a (100) GaAs semi-insulating substrate were prepared. Sample A was grown in situ using a Varian Gen II solid-source MBE system and sample B was deposited using a conventional E-gun evaporator (ULVAC EBX-8C). Before the deposition of Al, an undoped 200-nm-thick GaAs buffer layer served as the template for both samples. Sample A was then kept in the UHV MBE chamber to prevent the GaAs surface from oxidation. After the growth chamber was pumped down to 3×10^{-10} Torr to eliminate residual arsenic vapor pressure, an Al thin film was grown at $\sim 0\,^{\circ}\mathrm{C}$ at a rate of 0.18 μm/h (0.05 nm/s). Sample B with the same template was unavoidably exposed to air before it was loaded into a separate E-gun evaporation chamber. Although deoxidation using buffer-oxide etching (BOE) for 30 s was performed, we expected a thin native oxide to form on the GaAs surface before Al deposition. After pumping down the E-gun

 © 2013 The Japan Society of Applied Physics

chamber to less than 3×10^{-6} Torr, the Al film of sample B was evaporated at room temperature at a rate of about 0.72 µm/h (0.2 nm/s).

The structural properties of the two samples were analyzed with the Bede D1 high-resolution XRD system. The XRD setup is illustrated schematically in Fig. 1(a). The sample was placed on the x–y plane; the X-ray incident plane was the x–z plane with an incident angle of ω and a detection angle of 2θ. To prevent strong signal counts being observed from the 350-µm-thick GaAs substrate, low-incident-angle ($\omega = 0.5°$) 2θ scanning was performed. Moreover, two kinds of sample rotation were used to study the single-crystalline properties of the samples. χ rotation (x-axis rotation) was used to obtain the constructive X-ray interference of a specific lattice plane, and φ scanning (z-axis rotation) was carried out to confirm the single-crystalline quality of the sample.

Normal incident reflectivity spectra were taken using a commercial n&k analyzer (Filmetrics n&k 1500) at room temperature. The wavelength range and spot diameter are 190–1000 nm and 1 mm, respectively. For electrical resistivity and Hall measurements, both Al samples were processed into 80-µm-wide Hall bars by standard photolithography followed by chemical wet etching using BOE. The width-to-length ratio of the obtained Hall bars is about 1 : 8. Contact pads were fabricated using Ti/Au (30/150 nm) by E-gun evaporation and a lift-off method. The finished Hall-bar devices were wire-bonded on a ceramic chip carrier and attached on a variable temperature insert for measurements at low temperatures and high magnetic fields of up to 14 T. The electrical resistivity and Hall measurements were performed with a standard low frequency (87 Hz) lock-in technique. We use the four-probe method with a testing current of 1 mA. To avoid the superconductivity effect in Al, whose critical temperature is about 1.2 K, all the electrical measurements were performed at 4 K or higher.

3. Results and Discussion

The results of the XRD analysis of the two samples are shown in Figs. 1(b) and 1(c). In Fig. 1(b), with the low-incident-angle 2θ scanning of sample A with $\chi = -53°$ and $\varphi = 23°$, a single strong peak from Al(111) is observed. However, for sample B with $\chi = 0°$ and $\varphi = 0°$ under the same measurement conditions, multiple diffraction peaks are observed, as shown in Fig. 1(c). The observation of multiple peaks exhibits that sample B is a polycrystalline film. Note that the peak intensity of sample A is two orders stronger than that of sample B, indicating a highly ordered structure of sample A. The specific rotation angles ($\chi = -53°$, $\varphi = 23°$, and $2\theta = 39°$) also indicate that the Al(100) plane is perpendicular to the growth direction, i.e., GaAs(100) with a 45° rotation with the GaAs substrate, which is consistent with the observation by Cho and Dernier.[13] The XRD data show that the lattice constant of a face-centered cubic Al film is 0.4051 nm, which is very close to the bulk value (0.4049 nm); thus, the Al film is totally relaxed. To further confirm the single-crystalline structure of sample A, we performed φ-dependent scanning with the nonsymmetrical Al(111) axis aligned with the z-axis. As we can see in the inset of Fig. 1(b), the Al(111) peak of sample A is highly φ-dependent, with a full-width of half-maximum of ~0.5°.

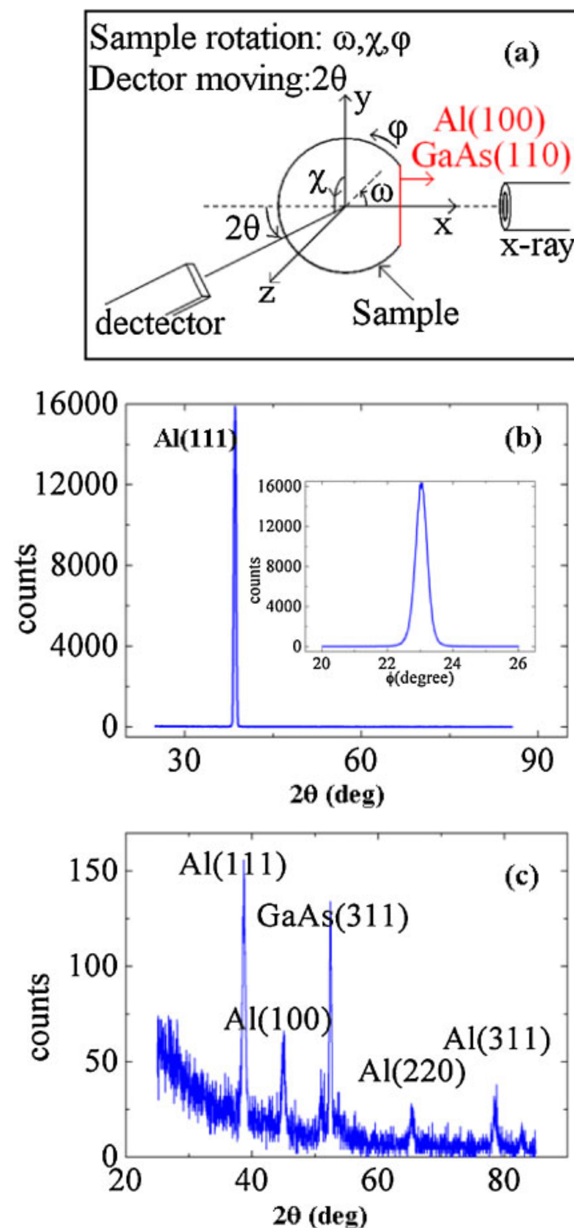

Fig. 1. (Color online) (a) Schematic setup of 2θ scanning XRD. Measured results of (b) sample A and (c) sample B. The inset of (b) shows the φ scanning of the Al(111) peak of sample A.

This reveals that sample A is indeed single-crystalline. We also measured the surface morphology of both samples in air with an AFM system (Veeco DI-3000). Typical $1 \times 1\,\mu m^2$ AFM images are shown in Fig. 2. Clearly, in Fig. 2(a), sample A has a smoother surface and its morphology shows a particular pattern that comes from the GaAs template underneath. In contrast, the surface image of sample B in Fig. 2(b) is rough and island-like, which has been commonly observed in previous studies.[1] From the results in Fig. 2, the surface roughness of sample A (sample B) was about 3.6 nm (7.5 nm). In all the studied samples, although the roughness varies from one sample to another, the MBE-grown ones always have a smoother surface morphology than those grown using the E-gun evaporator of the same thickness. The smallest roughness among all the MBE-grown samples is about 0.4 nm.

 © 2013 The Japan Society of Applied Physics

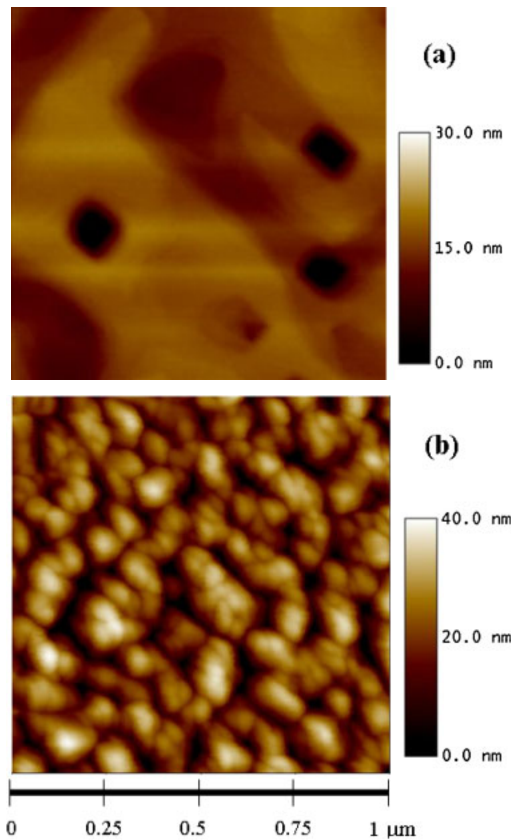

Fig. 2. (Color online) $1 \times 1\,\mu m^2$ AFM images of (a) sample A and (b) sample B.

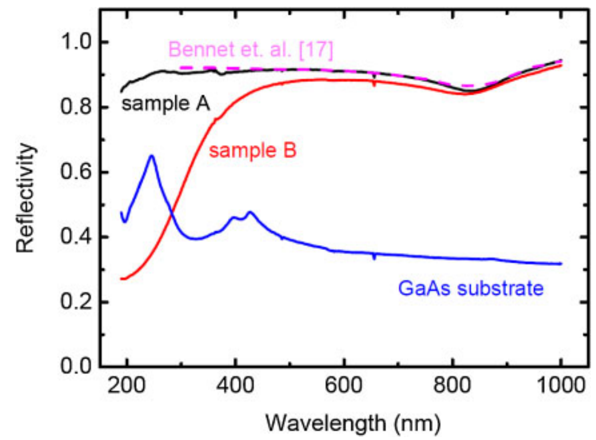

Fig. 3. (Color online) Measured optical reflectivity spectra of both samples and reference GaAs substrate. The spectra cited from Ref. 17 are also plotted (dash line).

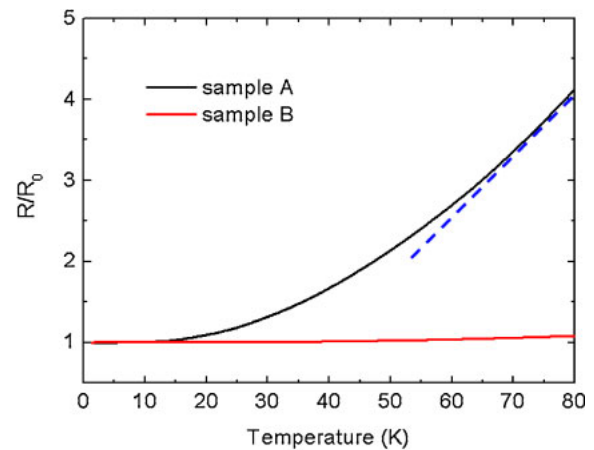

Fig. 4. (Color online) Temperature-dependent electrical resistivities of both samples. The dashed line shows the linear dependence of sample A at $T > 70\,K$.

The measured reflectivity spectra of both samples are plotted in Fig. 3 together with that of the reference sample, i.e., a bare GaAs substrate. For sample A, the reflectivity is nearly 90% in the range of 200–1000 nm except for the absorption dip at approximately 820 nm, which comes from the interband transition of Al.[17] On the other hand, the reflectivity of sample B is lower than that of sample A in the entire range and falls rapidly when the wavelength is shorter than about 400 nm. This clear difference in reflectivity in the ultraviolet (UV) range is observed in all the studied samples, which could be attributed to the higher roughness of the E-gun-evaporated samples. The high reflectivity in the UV regime reveals that MBE-grown Al thin films can serve as a highly reflective mirror for UV-based optoelectronic devices. Note that the small dips around 480 and 650 nm are not related to Al as they appear in the spectra of the bare GaAs substrate as well. Our result is quite consistent with that cited from Ref. 17, as plotted in Fig. 3.

We expected to see a clear difference in the electrical measurements between the two samples because the transport properties are significantly affected by the crystal structure. By using the method mentioned above, the measured resistivities of sample A at 4 and 300 K are 1.46×10^{-9} and $2.97 \times 10^{-8}\,\Omega\,m$, respectively. For sample B, the corresponding values are 8.89×10^{-8} and $1.69 \times 10^{-7}\,\Omega\,m$. At 4 K, the resistivity of sample A is two orders lower than that of sample B. As a result, the residue-resistance ratios (RRR) defined as R_{300K}/R_{4K} are 20.3 for sample A and 1.90 for sample B. These results evidence the superior crystal quality of sample A grown by MBE. In Fig. 4, we show the normalized resistivities $[R(T)/R(4\,K)]$ of both samples in the temperature range of 4–80 K. Commonly, the resistivity of Al films follows the following relation at low temperatures:[6,7,18)]

$$\rho(T) = \rho_0 + \alpha T^2 + \beta T^5. \quad (1)$$

The T^2 term comes from an electron–electron interaction and the T^5 dependence is caused by an electron-phonon interaction. The temperature-independent term ρ_0, which can be easily obtained as low-temperature limit resistivity, is dominated by temperature-independent scattering, such as defects, impurities, and boundary scattering. However, the data in Fig. 4 cannot be well fitted to Eq. (1). A detailed discussion about the temperature-dependent and superconductive characteristics is given elsewhere.[19,20] Here, we would like to note that, first, the residue resistivity ρ_0 of sample A is much larger than that of a high-purity bulk sample, which is about $10^{-11}\,\Omega\,m$ or less. This can be explained by the fact that the sample thickness is much smaller than the carrier mean free path and so the low-temperature resistivity is limited by the size effect. Second,

 © 2013 The Japan Society of Applied Physics

the temperature dependences of both samples become linear for $T > 70\,\mathrm{K}$ up to room temperature. Clearly, compared with sample B, sample A has a much larger temperature coefficient of resistance (TCR) which is defined as $[1/R(T)](dR/dT)$ (see the dash line in Fig. 4). The TCR at 80 K is about 1.94%/K (0.22%/K) for sample A (sample B). The large TCR of sample A is due to the reduced temperature-insensitive resistance caused by grain boundary and impurity scatterings. Therefore, single-crystalline Al films could also serve as highly-conductive temperature-sensing materials.

The longitudinal magnetoresistance (MR; defined as $\Delta\rho/\rho \equiv [\rho(B) - \rho(0)]/\rho(0)$) and transverse magnetoresistance (Hall resistance) were measured for the two samples under the perpendicular magnetic fields of 0–14 T at 4 K. As shown in Fig. 5(a), with increasing magnetic field, a significant increase in MR is observed in sample A. The resistance at 14 T is about 2.5 times larger than that at zero magnetic field. However, the corresponding MR of sample B is only about 1%, 2 orders smaller than that of sample A. One of the key factors of the magnetic field effect on transport properties, such as MR and Hall resistance, is $\omega_c\tau$. Here, ω_c is the cyclotron frequency proportional to magnetic strength and τ is the mean free time of carriers. It is widely accepted that, with a nonspherical Fermi energy surface, a larger $\omega_c\tau$ usually gives a larger MR[21] because a longer mean free time means that the magnetic field can affect the transport more significantly between collisions. Sample A has a much larger MR than sample B because its mean free time τ is much longer. On the other hand, the Hall measurement results of both samples are shown in Fig. 5(b). It is interesting that the Hall coefficient of sample A shows a transition from negative to positive as the magnetic field increases [see the inset of Fig. 5(b)]. The sign change is due to the special band structure in Al that has two partially filled Brillouin zones (second and third zones). The electrons in the second zone are hole-like, but those in the third zone are electron-like. Because the mean free time of electron-like carriers is longer than that of hole-like ones, the Hall resistance at low fields is contributed by electron-like carriers in the third zone. With increasing magnetic field, hole-like carriers take over as their population is higher. A similar behavior has been observed in high-quality bulk Al, but our result was the first observation in nanoscale Al thin films.[8] The sign change of Hall resistivity in bulk Al has also been analytically explained by the multiple-band theory.[22,23] In contrast, the Hall coefficient of sample B is always negative in our measurement range owing to its short mean free time of carriers.[23]

As noted earlier, the size effect dominates the transport properties of our Al thin film. To account for the size effect of thin films, Sondheimer derived analytical formulas for calculating the transport parameters, including resistivity, MR, and Hall resistivity, from their bulk values.[24] By using his theory, we perform a simple quantitative calculation to understand the size effect in sample A. We take the measured zero-magnetic-field resistivity to deduce the bulk resistivities for various p values. The parameter p is called the reflection parameter, representing the fraction of carriers arriving at the surface of thin films to be elastically reflected. With the bulk resistivity and the experimental MR and Hall

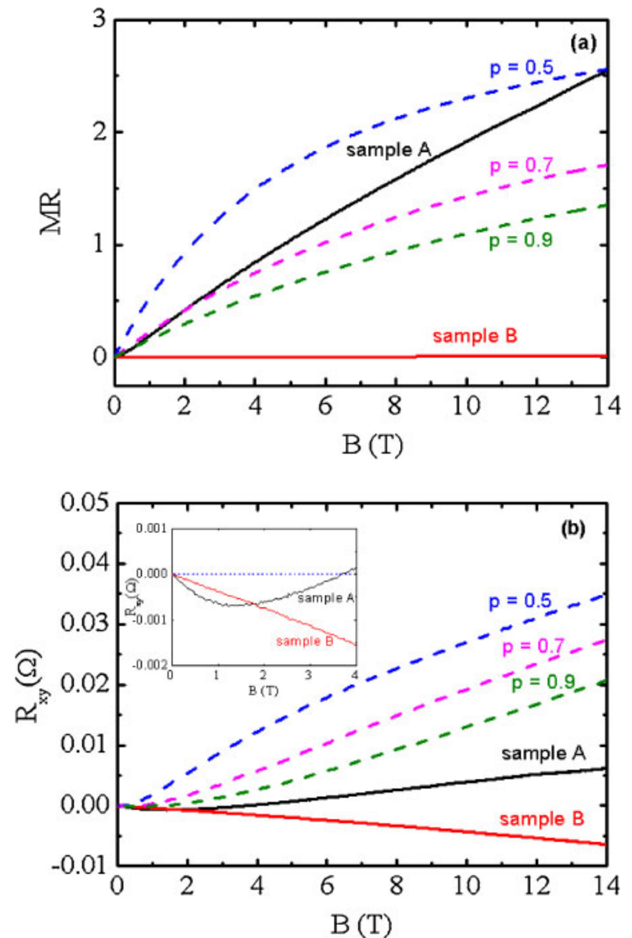

Fig. 5. (Color online) Measured (a) MR and (b) Hall resistances of both samples. The theoretical simulation results of sample A for the reflection parameter $p = 0.5$, 0.7, and 0.9 are also plotted. The inset shows the enlarged R_{xy} vs magnetic field B in the low-field regime.

data of bulk Al reported in Refs. 3 and 8, we calculate the MR and Hall resistivity of our 60-nm-thick Al film. The results are also plotted in Fig. 5 for $p = 0.5$, 0.7, and 0.9. Although the trend shows that the size effect plays a role in the transport properties of the thin film, a quantitative disagreement is revealed regardless of chosen p. Other scattering sources such as surface roughness, strain deformation, and Al/GaAs interface states or anisotropic scattering mechanisms have not been taken into account; therefore, further investigations are required to resolve this issue.

4. Conclusions

We have presented the characterization of Al thin films grown on a GaAs(100) substrate by MBE and using an E-gun evaporator. A single-crystalline Al film has been successfully formed by in situ MBE. The XRD data, reflectivity spectra, and electrical measurements clearly show that the Al film grown by MBE is of better quality than its counterpart. In comparison with the polycrystalline sample evaporated using an E-gun, the MBE-grown one shows an extremely low residue resistance, a high TCR, a high MR, and a bulk-like electron-to-hole transition of Hall resistivity. The optical reflectivity of the high-quality Al film reveals its potential applications in the fields of plasmonics and nanophotonics.

© 2013 The Japan Society of Applied Physics

Acknowledgements

This work was financially supported by the NSC and by the ATU Program of MOE in Taiwan. We thank the Center of Nano Science and Technology at National Chiao Tung University and the High-Magnetic Low-Temperature Laboratory at the National Device Laboratory for their equipment support. SWL would like to thank Y. M. Lin and C. H. Pan for their fruitful discussions and kind help on thin-film growth.

1) R. J. M. van Vucht, H. van Kempen, and P. Wyder: Rep. Prog. Phys. **48** (1985) 853.
2) K. Førsvoll and I. Holwech: J. Appl. Phys. **34** (1963) 2230.
3) R. J. Balcombe: Proc. R. Soc. London, Ser. A **275** (1963) 113.
4) K. Førsvoll and I. Holwech: Philos. Mag. **10** (1964) 921.
5) A. von Bassewitz and E. N. Mitchell: Phys. Rev. **182** (1969) 712.
6) J. C. Garland and D. J. Van Harlingen: J. Phys. F **8** (1978) 117.
7) J. R. Sambles, K. C. Elsom, and G. Sharp-Dent: J. Phys. F **11** (1981) 1075.
8) K. Yonemitsu, H. Sato, I. Sakamoto, and M. Fukuhara: J. Low Temp. Phys. **56** (1984) 267.
9) E. J. R. Vesseur, R. de Waele, H. J. Lezec, H. A. Atwater, F. J. García de Abajo, and A. Polman: Appl. Phys. Lett. **92** (2008) 083110.
10) J. S. Huang, V. Callegari, P. Geisler, C. Brüning, J. Kern, J. C. Prangsma, X. Wu, T. Feichtner, J. Ziegler, P. Weinmann, M. Kamp, A. Forchel, P. Biagioni, U. Sennhauser, and B. Hecht: Nat. Commun. **1** (2010) 150.
11) Y. J. Lu, J. Kim, H. Y. Chen, C. Wu, N. Dabidian, C. E. Sanders, C. Y. Wang, M. Y. Lu, B. H. Li, X. Qiu, W. H. Chang, L. J. Chen, G. Shvets, C. K. Shih, and S. Gwo: Science **337** (2012) 450.
12) R. Ludeke, L. L. Chang, and L. Esaki: Appl. Phys. Lett. **23** (1973) 201.
13) A. Y. Cho and P. D. Dernier: J. Appl. Phys. **49** (1978) 3328.
14) P. M. Petroff, L. C. Feldman, A. Y. Cho, and R. S. Williams: J. Appl. Phys. **52** (1981) 7317.
15) H. Nakahara, H. Matuhata, Y. Okada, T. Kurosu, M. Iida, and T. Yao: Appl. Phys. Lett. **58** (1991) 1970.
16) H. F. Liu, S. J. Chua, and N. Xiang: J. Appl. Phys. **101** (2007) 053510.
17) H. E. Bennett, M. Silver, and E. J. Ashley: J. Opt. Soc. Am. **53** (1963) 1089.
18) J. R. Sambles and K. C. Elsom: J. Phys. F **15** (1985) 161.
19) S. T. Lo, C. Chuang, S. D. Lin, K. Y. Chen, C.-T. Liang, S. W. Lin, J. Y. Wu, and M. R. Yeh: Nanoscale Res. Lett. **6** (2011) 102.
20) C. T. Liang, M. R. Yeh, S. D. Lin, S. W. Lin, J. Y. Wu, T. L. Lin, and K. Y. Chen: Chin. J. Phys. **50** (2012) 638.
21) A. B. Pippard: *Magnetoresistance in Metal* (Cambridge University Press, Cambridge, U.K., 1989) p. 1.
22) N. C. Banik and A. W. Overhauser: Phys. Rev. B **18** (1978) 1521.
23) N. W. Ashcroft and N. D. Mermin: *Solid State Physics* (Brooks/Cole, Independence, KY, 1976) p. 233.
24) E. H. Sondheimer: Phys. Rev. **80** (1950) 401.

© 2013 The Japan Society of Applied Physics